J|A|C|S
ARTICLES
Published on Web 05/25/2006

A High-Frequency EPR Study of Frozen Solutions of Gd^{III} Complexes: Straightforward Determination of the Zero-Field Splitting Parameters and Simulation of the NMRD Profiles

Meriem Benmelouka,[§] Johan Van Tol,[†] Alain Borel,[§] Marc Port,[‡] Lothar Helm,*[,§] Louis Claude Brunel,[†] and André E. Merbach[§]

Contribution from the Laboratoire de Chimie Inorganique et Bioinorganique, Ecole Polytechnique Fédérale de Lausanne, EPFL-BCH, CH-1015 Lausanne, Switzerland, National High Magnetic Field Laboratory, Center for Interdisciplinary Magnetic Resonance, Florida State University, Tallahassee, Florida, and Research Department, Guerbet, 95943 Roissy Cdg Cedex, France

Received December 20, 2005; E-mail: lothar.helm@epfl.ch

Abstract: Gd(III) ($S = {}^7/_2$) polyaminocarboxylates, used as contrast agents for Magnetic Resonance Imaging (MRI), were studied in frozen solutions by High-Frequency−High-Field Electron Paramagnetic Resonance (HF-EPR). EPR spectra recorded at 240 GHz and temperatures below 150 K allowed the direct and straightforward determination of parameters governing the strength of zero-field splitting (ZFS). For the first time, a correlation has been established between the sign of the axial ZFS parameter, *D*, and the nature of the chelating ligand in Gd(III) complexes: positive and negative signs have been observed for acyclic and macrocyclic complexes, respectively. Furthermore, it has been shown that complexes of the less symmetric acyclic DTPA derivatives possess a substantial rhombicity, *E*, in contrast to the more symmetric macrocyclic DOTA derivatives, where *E* is negligible. The results obtained are compatible with recent results of liquid-state EPR and allowed to simulate ^{1}H Nuclear Magnetic Relaxation Dispersion (NMRD) profiles with more directly physically meaningful EPR and NMR parameters over the full frequency range from 0.01 to 50 MHz.

Introduction

Ever since Paul C. Lauterbur (USA) and Sir Peter Mansfield (UK) invented Magnetic Resonance Imaging (MRI) in the 1970s,[1,2] this technique has become an increasingly powerful tool for medical diagnosis. Indeed this method is noninvasive and devoid of serious health hazards; only patients with metal or pacemakers inside their bodies may not be examined due to the intense magnetic field. For this resounding success, Lauterbur and Mansfield shared the Nobel Prize in Medicine for 2003. However, the technological developments of the last three decades are not yet sufficient to satisfy the demands of all radiological examinations. To shorten the examination time or to increase the image quality, physicians often use drugs known as *contrast agents*. Usually, these agents are paramagnetic Gd(III) complexes that induce an enhancement of the relaxation rate of the neighboring water protons (*relaxivity*) due to stochastic changes of the dipolar interaction with the unpaired electrons of the metal ion.[3] Several phenomena act as simultaneous modulation processes: (1) the rotational diffusion of the complex, described by a correlation time τ_R; (2) chemical exchange of the water molecules directly bound to the metal with the bulk (residence time τ_m);[4,5] and (3) the electronic spin relaxation, often described by the longitudinal and transverse relaxation times T_{1e} and T_{2e}. While it is well-known that the rotational diffusion coefficient is a function of the molecular size[6−8] and that the water exchange rate can be controlled to some extent by designing ligands with suitable steric constraints,[9,10] the electronic spin relaxation of Gd(III) complexes relevant for MRI remains the subject of much discussion.[11−16]

[§] Ecole Polytechnique Fédérale de Lausanne.
[†] Florida State University.
[‡] Guerbet.

(1) Lauterbur, P. G. *Nature* **1973**, *242*, 190.
(2) Mansfield, P. *J. Phys. C Solid State Phys.* **1977**, *10*, L55.
(3) (a) Merbach, A. E.; Tóth, É. *The Chemistry of Contrast Agents in Medical Magnetic Resonance Imaging*; John Wiley & Sons: Chichester, UK, 2001. (b) Kowalewski, J.; Kruk, D.; Parigi, J. *Adv. Inorg. Chem.* **2005**, *57*, 42.
(4) Helm, L.; Merbach, A. E. *Chem. Rev.* **2005**, *105*, 1923.
(5) Helm, L. G.; Nicolle, M.; Merbach, A. E. *Adv. Inorg. Chem.* **2005**, *57*, 327.
(6) Tóth, É.; Pubanz, D.; Vauthey, S.; Helm, L.; Merbach, A. E. *Chem. Eur. J.* **1996**, *2*, 1607.
(7) Caravan, P.; Greenfield, M. T.; Li, X. D.; Sherry, A. D. *Inorg. Chem.* **2001**, *40*, 6580.
(8) Nicolle, G. M.; Tóth, É.; Eisenwiener, K.-P.; Macke, H. R.; Merbach, A. E. *J. Biol. Inorg. Chem.* **2002**, *7*, 757.
(9) Laus, S.; Ruloff, R.; Tóth, É.; Merbach, A. E. *Chem. Eur. J.* **2003**, *9*, 3555.
(10) Jaszberenyi, Z.; Sour, A.; Tóth, É.; Benmelouka, M.; Merbach, A. E. *Dalton Trans.* **2005**, *16*, 2713−2719.
(11) Strandberg, E.; Westlund, P.-O. *J. Magn. Reson. A* **1996**, *122*, 179.
(12) Clarkson, R. B.; Smirnov, A. I.; Smirnova, T. I.; Kang, H.; Belford, R. L.; Earle, K.; Freed, J. H. *Mol. Phys.* **1998**, *96*, 1325.
(13) Rast, S.; Fries, P. H.; Belorizky, E. *J. Chem. Phys.* **2000**, *113*, 8724.
(14) Nilsson, T.; Kowalewski, J. *Mol. Phys.* **2000**, *98*, 1617.
(15) Rast, S.; Fries, P. H.; Belorizky, E.; Borel, A.; Helm, L.; Merbach, A. E. *J. Chem. Phys.* **2001**, *115*, 7554.
(16) Kruk, D.; Nilsson, T.; Kowalewski, J. *Phys. Chem. Chem. Phys.* **2001**, *3*, 4907.

Since the $^8S_{7/2}$ ground state of the Gd(III) ion is well-known to undergo zero-field splitting in the solid state,[17,18] Hudson and Lewis proposed a basic theory of the EPR line shape of Gd(III) complexes in solution assuming a transient zero-field splitting (ZFS), modulated by rotation or molecular distortions as the main relaxation mechanism.[19] On the basis of this model, transverse and longitudinal relaxation matrices can be derived using the approach of Redfield.[20] In general, the zero-field splitting (ZFS) lifts the degeneracy of the electronic spin levels of transition metal compounds when the system deviates from a spherical symmetry.[21] Rast et al.[13,22] recognized that even highly symmetrical complexes, such as the aqua ion $[Gd(H_2O)_8]^{3+}$ (point group D_{4h}), have a permanent nonzero ZFS and developed a refined model of the electron spin relaxation of the *S* state metal ion complexes in solutions. This refined treatment includes a contribution of the rotational modulation of the static (i.e., average) crystal field surrounding the Gd(III) through molecular tumbling as well as the usual transient ZFS caused by vibrations, intramolecular rearrangements, and collisions with surrounding solvent molecules. Thus, one can say that, for Gd(III) ions, the structure and dynamics of the electronic density of the chelate framework surrounding the metal determine the ZFS and therefore the electron spin relaxation rates in solution. A better knowledge of the ZFS parameters of MRI contrast agents and their relationship to chelate structure and environment is necessary to establish a structure−function relationship for rational contrast agent design.

Extensive experimental data are usually required to determine accurately the underlying parameters (ZFS magnitude and correlation times). For small complexes, such as the octa aqua ion[4] or low molecular weight chelates,[12,23] the analysis of EPR measurements in aqueous solution at multiple frequencies and temperatures yielded parameters compatible with ^{1}H and ^{17}O NMR relaxation data. Furthermore, the combination of the static and transient crystal field effects was able to correctly predict the longitudinal relaxation times observed experimentally using the Longitudinally Detected EPR (LODEPR) method.[24] However, the analysis of EPR spectra of slow-rotating molecules is not as straightforward, as the Redfield approximations are not valid for such compounds. For these systems, calculating the EPR line shape becomes more tedious and requires computationally expensive methods, such as Monte Carlo spin dynamics[15,25] or solving the stochastic Liouville equation,[26−28] as well as a deeper knowledge of the spin Hamiltonian and its associated dynamics.[29−31] To obtain such information, it is necessary to follow a different approach in order to study independently the parameters of interest. For example, the fluctuations of the lanthanide(III) coordination polyhedron have been studied using molecular dynamics simulations.[32,33] Alternatively, Fries and collaborators developed an elegant method to determine the effective longitudinal electronic relaxation time T_{1e} in solution, based on outer sphere nuclear relaxation of noninteracting solute probes using commercial fast field-cycling NMR relaxometers. This method gives an effective longitudinal relaxation time but no direct information on the ZFS.[34,35] In this paper, we address another side of the problem, namely, the ZFS itself. Traditionally, solid-state EPR has been the method of choice for the direct study of the electron spin Hamiltonian, with the possibility to determine all components of the *g*-, *A*-, and ZFS tensors.[36] However, to be meaningful for the spin relaxation in liquids, a precise relationship between the solid state and solution parameters must be established. The models where a permanent nonzero ZFS is present[13,22,27−29,37] are much better in this respect. In particular, Rast's[15,38] model describes the transient ZFS modulation using an Ornstein−Uhlenbeck process,[39] namely, random jumps around an average value with a Gaussian probability distribution. This process is actually a dynamical equivalent to the *strain* encountered in the analysis of disordered solid-state EPR spectra.[40,41] Gaussian strain is a phenomenological description of a distribution of the spin Hamiltonian parameters throughout the sample, for example, due to differences in the hydrogen bonding pattern around the spins. This model can be applied to the *g*-factor[42−44] (*g*-strain) and hyperfine coupling[45,46] (*A*-strain), as well as to the ZFS tensor[47−49] (*D*, *E*-strain). The formal equivalence of the strain and the transient ZFS means that the determination of the strain parameters of the ZFS and their associated strains in the solid state provides us with an independent access to the key factors governing electron spin relaxation. Even the sign of the ZFS parameters can be determined through measurements at very low temperatures (<10 K) and high EPR frequencies. Of course, the method is applicable to molecules of arbitrary size since rotational motion plays no role in this case. Furthermore, we can expect a similar disorder in a frozen glass as in a liquid. Thus we can

(17) Misra, S. K. In *Handbook of Electron Spin Resonance*; Poole, C. P. J., Farach, H. A., Eds.; Springer: New York, 1999; Vol. 2, p 257.
(18) Misra, S. K. In *Handbook of Electron Spin Resonance*; Poole, C. P. J., Farach, H. A., Eds.; Springer: New York, 1999; Vol. 2, p 99.
(19) Hudson, A.; Lewis, J. W. E. *Trans. Faraday Soc.* **1970**, *66*, 1297.
(20) Redfield, A. G. In *Advances in Magnetic Resonance*; Waugh, J. S., Ed.; Academic Press Inc.: New York, 1965; Vol. 1, p 1.
(21) Misra, S. K. In *Handbook of Electron Spin Resonance*; Poole, C. P. J., Farach, H. A., Eds.; Springer: New York, 1999; Vol. 2, p 115.
(22) Rast, S.; Borel, A.; Helm, L.; Belorizky, E.; Fries, P. H.; Merbach, A. E. *J. Am. Chem. Soc.* **2001**, *123*, 2637.
(23) Dunand, F. A.; Borel, A.; Helm, L. *Inorg. Chem. Commun.* **2002**, *5*, 811.
(24) Borel, A.; Helm, L.; Merbach, A. E.; Atsarksin, V. A.; Demidov, V. V.; Odintsov, B. M.; Belford, R. L.; Clarkson, R. B. *J. Phys. Chem. A* **2002**, *106*, 6229.
(25) Sharp, R.; Abernathy, S. M.; Lohr, L. L. *J. Chem. Phys.* **1997**, *107*, 7620.
(26) Freed, J. H.; Bruno, G. V.; Polnaszek, C. F. *J. Phys. Chem.* **1971**, *75*, 3385.
(27) Benetis, N.; Kowalewski, J.; Nordenskiöld, L.; Wennerström, H.; Westlund, P.-O. *Mol. Phys.* **1983**, *48*, 329.
(28) Usova, N.; Westlund, P.-O.; Fedchenia, I. I. *J. Chem. Phys.* **1995**, *103*, 96.
(29) Kruk, D.; Kowalewski, J.; Westlund, P.-O. *J. Chem. Phys.* **2004**, *121*, 2215.
(30) Borel, A.; Clarkson, R. B.; Belford, R. L. Submitted.
(31) Westlund, P.-O.; Zhou, X. *J. Magn. Reson.* **2005**, *173*, 75.
(32) Kowall, T.; Foglia, F.; Helm, L.; Merbach, A. E. *J. Phys. Chem.* **1995**, *99*, 13078.
(33) Yerly, F.; Borel, A.; Helm, L.; Merbach, A. E. *Chem. Eur. J.* **2003**, *9*, 5468.
(34) Fries, P. H.; Ferrante, G.; Belorizky, E.; Rast, S. *J. Chem. Phys.* **2003**, *119*, 8636.
(35) Fries, P. H.; Belorizky, E. *J. Am. Chem. Soc.* **2005**, *127*, 15801.
(36) Abragam, A.; Bleaney, B. *Electron Paramagnetic Resonance of Transition Ions*; University Press: Oxford, 1970.
(37) Zhou, X.; Caravan, P.; Clarkson, R. B.; Westlund, P.-O. *J. Magn. Reson.* **2004**, *167*, 147.
(38) Rast, S.; Fries, P. H.; Belorizky, E. *J. Chim. Phys.* **1999**, *96*, 1543.
(39) Uhlenbeck, G. E.; Ornstein, L. S. *Phys. Rev.* **1930**, *36*, 823.
(40) Froncisz, W.; Hyde, J. S. *J. Chem. Phys.* **1980**, *73*, 3123.
(41) Hagen, W. R.; Hearshen, D. O.; Sands, R. H.; Dunham, W. R. *J. Magn. Reson.* **1985**, *61*, 220.
(42) Cage, B.; Hassan, A. K.; Pardi, L.; Krzystek, J.; Brunel, L.-C.; Dalal, N. S. *J. Magn. Reson. A* **1997**, *124*, 495.
(43) Mustafi, D.; Galtseva, E. V.; Krystek, J.; Brunel, L.-C.; Makinen, M. W. *J. Phys. Chem. A* **1999**, *103*, 11279.
(44) Lassmann, G.; Kolberg, M.; Bleifuss, G.; Graslund, A.; Sjoberg, B. M.; Lubitz, W. *Phys. Chem. Chem. Phys.* **2003**, *5*, 2442.
(45) Cannistraro, S. *J. Phys. France* **1990**, *51*, 131.
(46) Venturelli, A.; Nilges, M. A.; Smirnov, A.; Belford, R. L.; Francesconi, L. C. *J. Chem. Soc., Dalton Trans.* **1999**, 301.
(47) George, G. N.; Prince, R. C.; Bare, R. E. *Inorg. Chem.* **1996**, *35*, 434.
(48) Pierik, A. J.; Hagen, W. R.; Dunham, W. R.; Sands, R. H. *Eur. J. Biochem.* **1992**, *206*, 705.
(49) Seidel, A. H.; Bill, E. L.; Nordblad, P.; Kilar, F. *Arch. Biochem. Biophys.* **1994**, *308*, 52.

Scheme 1. Acyclic Compounds

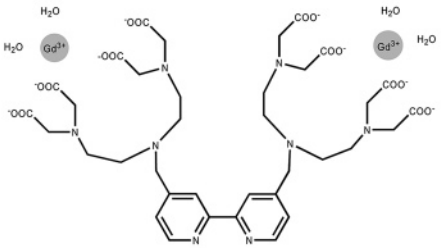

$[Gd_2(bipy\text{-}DTTA)(H_2O)_4]^{2-}$

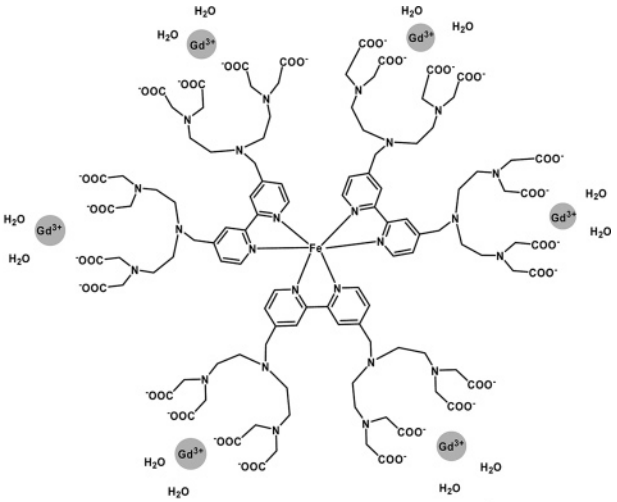

$[Fe\{[Gd_2(bipy\text{-}DTTA)(H_2O)_4]\}_3]^{4-}$

$[Gd_2M(tpy\text{-}DTTA)_2(H_2O)_4]$ (M^{II} = Fe^{II}, Ru^{II})

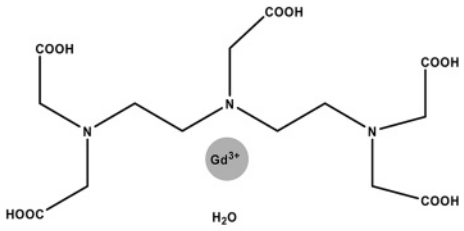

$[Gd(DTPA)(H_2O)]^{2-}$

use frozen samples to probe both the mean values of the ZFS tensor and their distributions, which we can then compare with the magnitude parameters obtained from relaxation studies of aqueous solutions.

In this paper, we report and analyze the EPR spectra of several Gd(III) chelates (Schemes 1 and 2) in water−glycerol glasses. The chelates include some well-known compounds already used for medical applications (DOTA, DTPA), as well as more recent molecules. The heterometallic, self-assembled Metallostar $[Fe\{[Gd_2(bipy\text{-}DTTA)(H_2O)_4]\}_3]^{4-}$ and its monomer $[Gd_2(bipy\text{-}DTTA)(H_2O)_4]^{2-}$ have been studied in its pure forms as well as in magnetic dilution with $[Fe\{[Y_2(bipy\text{-}DTTA)(H_2O)_4]\}_3]^{4-}$ and $[Y_2(bipy\text{-}DTTA)(H_2O)_4]^{2-}$, respectively (Scheme 1). Other self-assembled Gd(III) complexes studied were the dinuclear $[Gd_2M(tpy\text{-}DTTA)_2(H_2O)_4]$ with M = Fe^{II}, Ru^{II}. Two samples of Gd-P792 complexes, which are macromolecular DOTA derivatives, have been investigated. One sample contained Gd-P792(R) with six different stereoisomers determined by the configuration at each of the stereogenic centers at carbon: 4*R* (4*S*); *RSSS* (*SRRR*) and the achiral diastereoisomers *RSRS* and *RRSS*.[50] The second sample Gd-P792(B) had only the configuration 4*R* (4*S*) (Scheme 2). The last two complexes considered were the dinuclear complexes $[Gd_2(p/mX(DO3A)_2)(H_2O)_2]$. These ligands contain two $DO3A^{3-}$ metal chelating units on a xylene core as a noncoordinating linker in *meta* (*m*) and *para* (*p*) position.

Various aspects, such as the different conformations for the macrocyclic complexes, the metal−metal interaction in the binuclear complexes, and the influence of the *para* or *meta* substitution in the xylene derivative, are investigated.

Experimental Section

Materials. The Gd-P792 (R, B)[51] were supplied by Guerbet pharmaceuticals. Syntheses of $[Gd_2M(tpy\text{-}DTTA)_2(H_2O)_4]$ (M^{II} = Fe^{II}, Ru^{II}),[52] $[Gd_2(mX(DO3A)_2)(H_2O)_2]$, $[Gd_2(pX(DO3A)_2)(H_2O)_2]$,[53] $[Gd_2(bipy\text{-}DTTA)(H_2O)_4]^{2-}$, and $[Fe\{[Gd_2(bipy\text{-}DTTA)(H_2O)_4]\}_3]^{4-}$[54] have been described previously.

Sample Preparation. Most samples were prepared in situ by dissolution of the ligand (10% excess) in $Gd(ClO_4)_3$. The pH was adjusted to 6.5 by adding NaOH solution. Final concentrations of 5 mM for all glasses except for $[Gd(DOTA)(H_2O)]^-$ and $[Gd(DTPA)(H_2O)]^{2-}$ (0.5 mM) were prepared in 1:1 (v/v) glycerol/water solution. For $[Y_2/Gd_2(bipy\text{-}DTTA)(H_2O)_4]^{2-}$ and $[Fe\{Y_2/Gd_2(bipy\text{-}DTTA)(H_2O)_4\}_3]^{4-}$, the same process was followed by adding a mixed solution of 90% $Y(ClO_4)_3$ and 10% $Gd(ClO_4)_3$. The Gd-P792(B) and Gd-P792(R) solutions were prepared by dissolving a weighed amount of the complex in doubly distilled water. The pH of both samples was adjusted to 6.5. All solutions were checked for the absence of free Gd(III) ion using the xylenol orange test.[55]

EPR Measurements. The EPR spectra at 240 GHz were measured at the EPR facility of the National High Magnetic Field Laboratory with a home-built quasi-optical superheterodyne spectrometer.[56] A configuration without cavity was used, with a Teflon sample cup

(50) Vander Elst, L.; Raynal, I.; Port, M.; Tisnes, P.; Muller, R. N. *Eur. J. Inorg. Chem.* **2005**, 1142.

(51) Port, M.; Corot, C.; Rousseaux, O.; Raynal, I.; Devoldere, L.; Idée, J. M.; Dencausse, A. *Magn. Reson. Mater. Phys. Biol. Med.* **2001**, *12*, 121.
(52) Costa, J.; Ruloff, R.; Burai, L.; Helm, L.; Merbach, A. E. *J. Am. Chem. Soc.* **2005**, *127*, 5147.
(53) Costa, J.; Toth, E.; Helm, L.; Merbach, A. E. *Inorg. Chem.* **2005**, *44*, 4747.
(54) Livramento, J. B.; Toth, E.; Sour, A.; Borel, A.; Merbach, A. E.; Ruloff, R. *Angew. Chem., Int. Ed.* **2005**, *42*, 1480.
(55) Brunisholz, G.; Randin, M. *Helv. Chim. Acta* **1959**, *42*, 1927.
(56) Van Tol, J.; Brunel, L. C.; Wylde, R. J. *Rev. Sci. Instrum.* **2005**, *76*, 074101.

Scheme 2. Macrocyclic Compounds

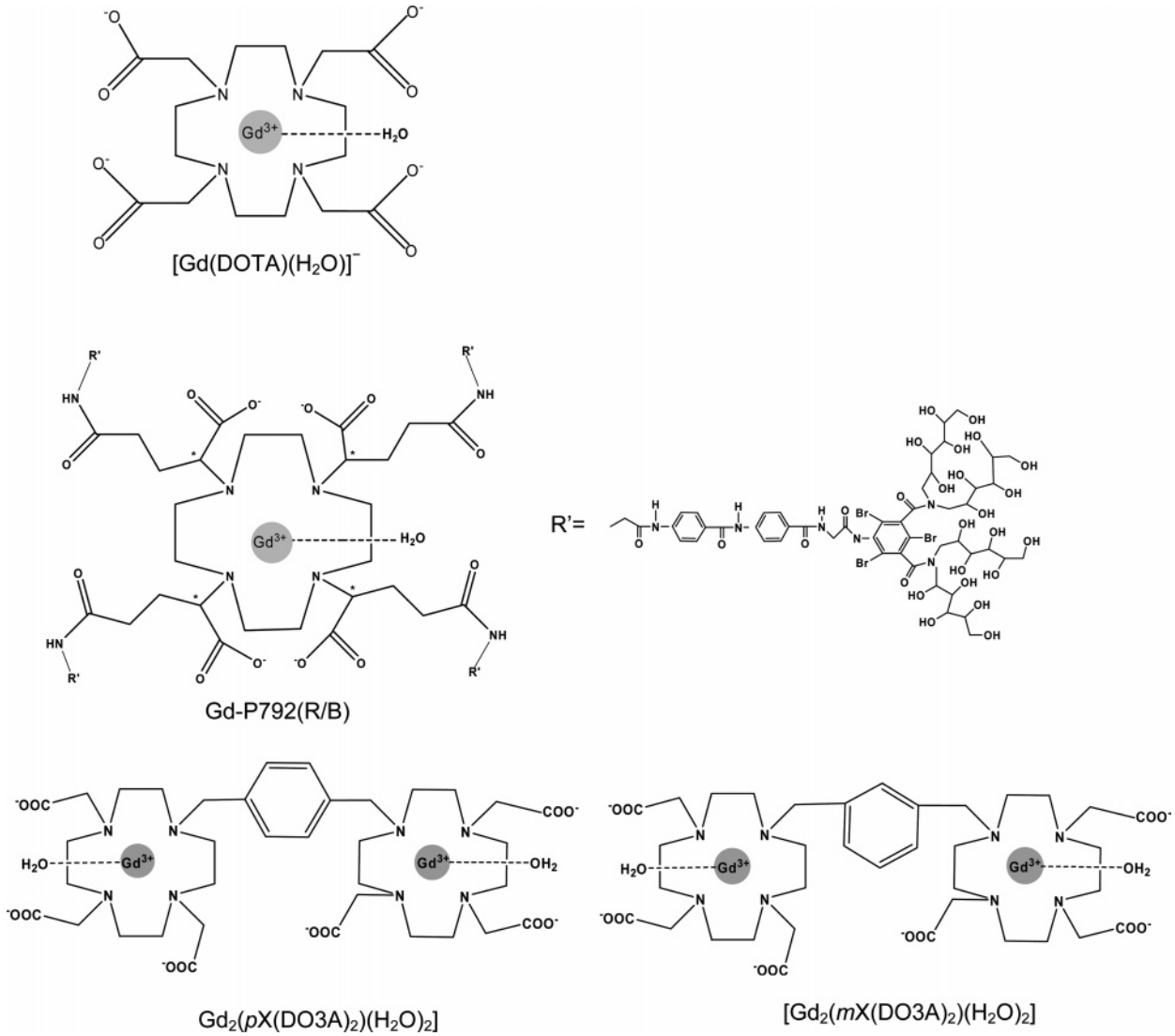

containing about 40 μL of the solution of the Gd(III) complex. Good glasses were formed by flash freezing the sample in liquid nitrogen before loading into the pre-cooled continuous-flow cryostat.

The photon energy of 240 GHz electromagnetic radiation corresponds to a temperature of 11.5 K. Therefore, at 4 K, only transitions between the lowest energy levels are observed. However, even at a very low irradiation power, with a B_1 field smaller than 1 μT, the spectrum was distorted due to saturation. For that reason, at the lowest temperatures, rapid-passage EPR[57] was employed to record the spectra, using relatively high power ($\sim$1 mW at the sample, $B_1 \sim 10$ μT) and small modulation amplitudes. Instead of a derivative line shape, the absorption line shape is directly obtained. At temperatures above 30 K, standard CW-EPR was used.

Data Analysis. The EPR spectra were simulated and fitted using a home-written program, EPRcalc,[58] which utilizes complete diagonalization of the effective spin Hamiltonian, which can be written as follows:

$$\hat{H} = \mu_B \hat{S} \cdot \vec{\vec{g}} \cdot \vec{B} + D(\hat{S}_z^2 - \hat{S}^2/3) + E(\hat{S}_x^2 - \hat{S}_y^2) \qquad (1)$$

with $S = {}^7/_2$. The first term represents the field-dependent electron Zeeman contribution, and the second and third terms, without any explicit B_0 dependence, represent the zero-field splitting. Higher order terms are neglected. The parameter $\vec{\vec{g}}$ is the Zeeman splitting tensor, μ_B the Bohr magneton, and B_0 the external magnetic field. D and E are the axial and rhombic ZFS coefficients, which describe the deviation from the octahedral and the axial symmetry, respectively. For simplicity, we assumed $\vec{\vec{g}}$ to be isotropic.

The distributions, in the frozen solution, of D and E are noted D-strain (σD) and E-strain (σE) and are assumed to be Gaussian and given by eq 2.

$$P(D_i) \sim e^{-(2(D_i - D)/\sigma D)^2};\ P(E_i) \sim e^{-(2(E_i - E)/\sigma E)^2} \qquad (2)$$

They are accounted for by including a Gaussian line-broadening that is proportional to the shift of the transitions due to a change in D and E. No correlation between σD and σE is assumed.

Results and Discussion

At high magnetic field, the Zeeman interaction energy becomes larger than the zero-field splitting (ZFS). By sweeping a large magnetic field range under irradiation with a high microwave frequency (up to 8.9 T and 240 GHz), additional transitions become observable in the spectrum.[59] This permits the determination of ZFS values larger than those accessible at standard X-band (0.33 T, 9.4 GHz) and Q-band (1.5 T, 35 GHz)

(57) Portis, A. M. *Phys. Rev.* **1955**, *100*, 1219.
(58) Van Tol, J. *EPRcalc*; National High Magnetic Field Laboratory, 2005.

frequencies. At higher magnetic field, the Zeeman term dominates the ZFS term in the spin Hamiltonian, and the high-frequency spectrum of a $S \geq {}^3/_2$ (half integer) system exhibits a sharp peak that can be easily assigned to the central transition $m_s = -1/2 \rightarrow +1/2$.

The magnitude of the zero-field splitting of the Gd(III) ($S = {}^7/_2$) complexes can be of the same order of magnitude as the X-band microwave energy (9.4 GHz). In this case, the spectrum analysis is not straightforward since the EPR spectra become very asymmetric. Thus, the use of very high-frequency EPR makes the analysis simpler and more reliable for Gd(III) ions.

At low temperature and high magnetic field, $k_BT \ll g_{iso}\mu_BB_0$, the spin polarization is increased and almost all spins are in the Zeeman ground state ($m_s = -7/2$). The intensity of the transition originating from this level (i.e., $m_s = -7/2 \rightarrow -5/2$) is then dramatically increased and forms a broad powder pattern which dominates the spectra. Nevertheless, the central transition ($m_s = -1/2 \rightarrow +1/2$) remains observable due to its narrow width. The relative position of this weak central transition with respect to the overall powder pattern provides us with an elegant way to determine the sign of the ZFS D parameter, as represented in Figure 1. If D is positive, the ground state at zero magnetic field is $\pm 1/2$ and the $-7/2 \rightarrow -5/2$ transition (**) for B_0 parallel to the axial direction of the ZFS occurs at a higher magnetic field than the sharp $-1/2 \rightarrow +1/2$ (*) transition in a continuous wave spectrum. If D is negative, the ground state is $\pm 7/2$ and the broad intense $-7/2 \rightarrow -5/2$ transition is observed at lower magnetic field than the sharp $-1/2 \rightarrow +1/2$ transition. In the case of the usual convention $|D| > 3|E|$, this means that, if the transition furthest from the central sharp feature occurs at high field, D is positive. If it occurs at low field, D is negative (Figure 1).

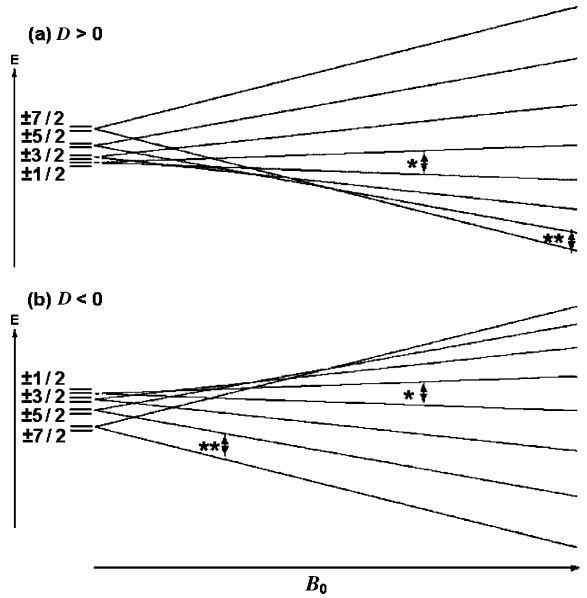

Figure 1. Schematic representation of energy levels with positive (a) and negative (b) D values. The $-7/2 \rightarrow -5/2$ (**) and $-1/2 \rightarrow +1/2$ (*) transitions for B_0 parallel to the axial direction of the ZFS are pointed out, showing their relative positions for both cases.

Figures 2 and 3 show selected experimental and calculated EPR spectra of selected Gd(III) complexes at 240 GHz and variable temperature. For all complexes, the rapid passage spectra at 4 K showed a broad line shape superposed with a small sharp peak that is hardly observable. The broad line is assigned to the transitions between the lower levels and the sharp peak to those of the central energy levels, respectively.

At 40 and 150 K, conventional absorption derivative spectra were obtained and, the sharp peak of the $m_s = -1/2 \rightarrow +1/2$ transition dominates the spectra.

The four ZFS parameters, D, E, σD, and σE, were determined from least-squares fitting of the 4 K spectra. As is customary, we divided the Gd(III) complexes into two groups, acyclic (Scheme 1) and macrocyclic (Scheme 2) compounds. The fitting results for the acyclic complexes can be found in Table 1, and those for the cyclic complexes are reported in Table 2. The validity of the ZFS parameters derived from 4 K spectra was then confirmed by their ability to simulate the higher temperature spectra (Figures 2 and 3). The calculated spectra are in good agreement with the experimental ones.

Comparing the data in Tables 1 and 2 reveals that the sign of D is positive for the acyclic complexes and negative for all cyclic complexes except Gd-P792(R). Although surprising, such a sign reversal between Gd(III) compounds with similar chemical environments is not without precedent in the literature. Misra et al. have determined a positive sign of D for Gd(III)-doped crystals of CeF_3, LaF_3, PrF_3, and NdF_3[60] and a negative one for Gd(III)$^-$doped crystals of $LiYF_4$.[61] Buckmaster has reported negative as well as positive signs of D for several examples of Gd(III) halides in different matrices.[62]

Acyclic Complexes. Despite a different coordination polyhedron for DTPA, compared to that of DTTA derivative complexes, very similar ZFS parameters (D, E, σD, and σE) were determined (Table 1). In addition, the nature of the linking bridge group attached to the DTTA chelating unit in $[Gd_2(bipy\text{-}DTTA)(H_2O)_4]^{2-}$ and $[Gd_2M(tpy\text{-}DTTA)_2(H_2O)_4]$ plays no apparent role. The nitrogen atoms of the DTTA moiety have different chemical properties in these complexes, as shown, for example, by the much lower pGd of $[Gd_2M(tpy\text{-}DTTA)_2(H_2O)_4]$ due to the strong electron-withdrawing character of the iron-(II)-complexed terpyridine unit in comparison with a methylene bridge in $[Gd_2(bipy\text{-}DTTA)(H_2O)_4]^{2-}$,[52] which could affect the ligand field acting on the 4f electrons of Gd(III). Nevertheless, the ZFS parameters for these two species are essentially the same.

As it was mentioned before, we observed a positive sign of D for the acyclic group of ligands studied. The sign of D is not related to obvious structural parameters of Gd(III) compounds. However, it is important to note that the sign of D is irrelevant to the electronic spin relaxation in solution because only the square of the ZFS parameters is involved in the equations. For all acyclic complexes, the rhombic parameter E is significantly larger than zero. This is expected regarding to the low symmetry of those compounds. σD and σE, the distribution of D and E, are unusually large compared to D and E themselves.

Concerning spin dilution with diamagnetic Y(III), for $[Gd_2(bipy\text{-}DTTA)(H_2O)_4]^{2-}$ ($r_{Gd-Gd} \geq 14$ Å)[63] and [Fe{[Gd_2(bipy-

(59) Chemerisov, S. D.; Grinberg, O. Ya.; Tipikin, D. S.; Lebedev, Ya. S.; Kurreck, H.; Möbius, K. *Chem. Phys. Lett.* **1994**, *218*, 353.
(60) Misra, S. K.; Mikolajczak, P.; Korczak, S. *J. Chem. Phys.* **1981**, *74*, 922.
(61) Misra, S. K.; Kahirizi, M.; Mikolajczak, P.; Misiak, L. *Phys. Rev.* **1985**, *B32*, 4738.
(62) Buckmaster, H. A. *Magn. Reson. Rev.* **1973**, *2*, 273.
(63) Livramento, J. B.; Sour, A.; Borel, A.; Merbach, A. E.; Tóth, É. *Chem. Eur. J.* **2006**, *12*, 989.

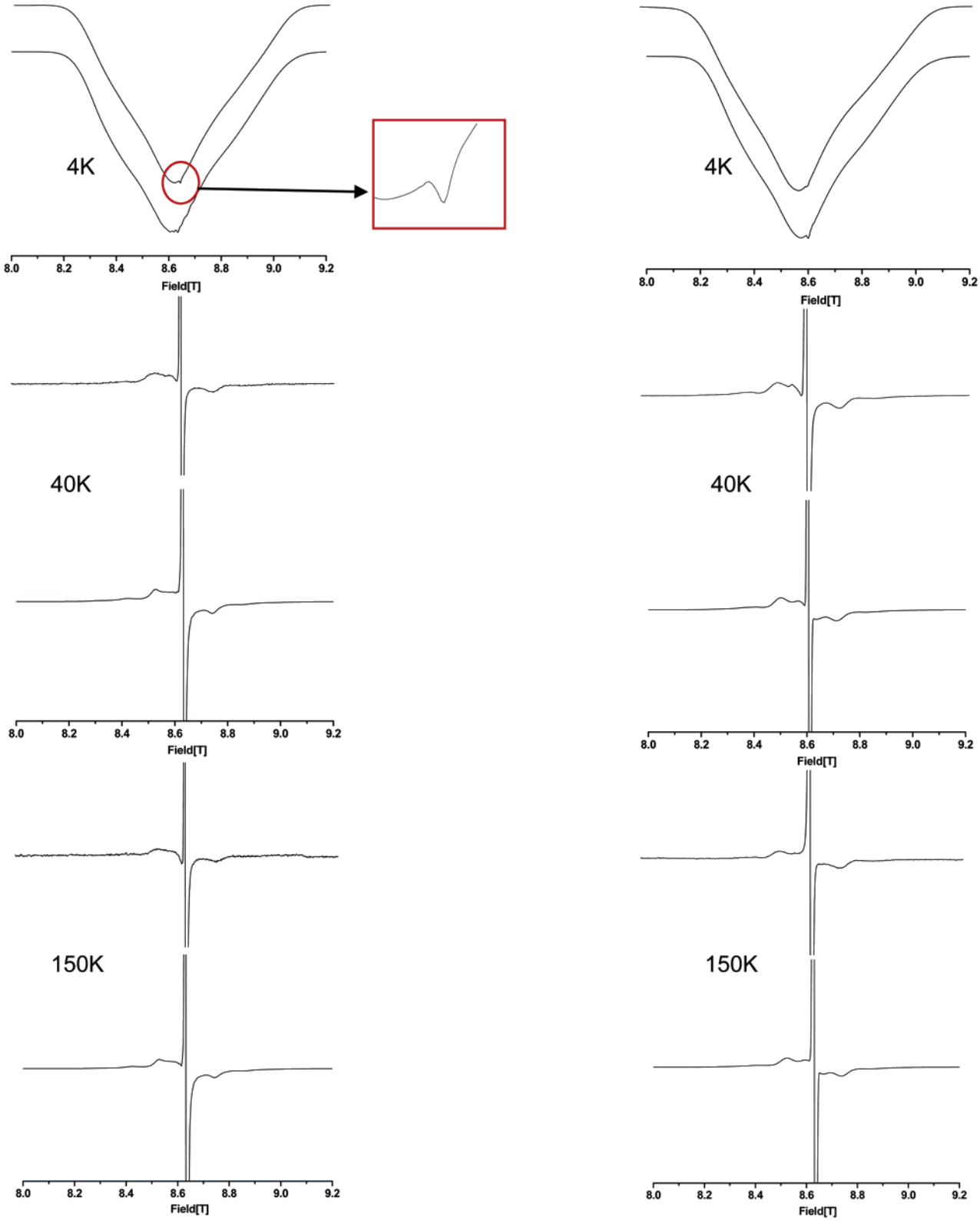

Figure 2. EPR spectra in water−glycerol glass for acyclic compounds at 4, 40, and 150 K: left, the experimental (upper) and the fitted (lower) spectra of $[Gd_2(bipy\text{-}DTTA)(H_2O)_4]^{2-}$ glass; right, the experimental (upper) and the fitted (lower) spectra of $[Fe\{[Gd_2(bipy\text{-}DTTA)(H_2O)_4]\}_3]^{4-}$ glass. The inset at 4 K shows the small $-1/2 \rightarrow +1/2$ transition.

DTTA)$(H_2O)_4]\}_3]^{4-}$, no variation in the ZFS parameters is observed. The change in the central metal ion from Fe(II) to Ru(II) in $[Gd_2M(tpy\text{-}DTTA)_2(H_2O)_4]$ ($r_{Gd-Gd} = 12.5$ Å)[52] does not contribute to a possible interaction between Gd(III) ions. Therefore, we can conclude that the interaction, if there is one, between Gd(III) centers in those binuclear complexes has no influence neither on the magnitude nor the sign of *D*, *E*, and their distributions.

Macrocyclic Complexes. We observe a negative sign of *D* for all macrocyclic compounds and a large *D*-strain which is of

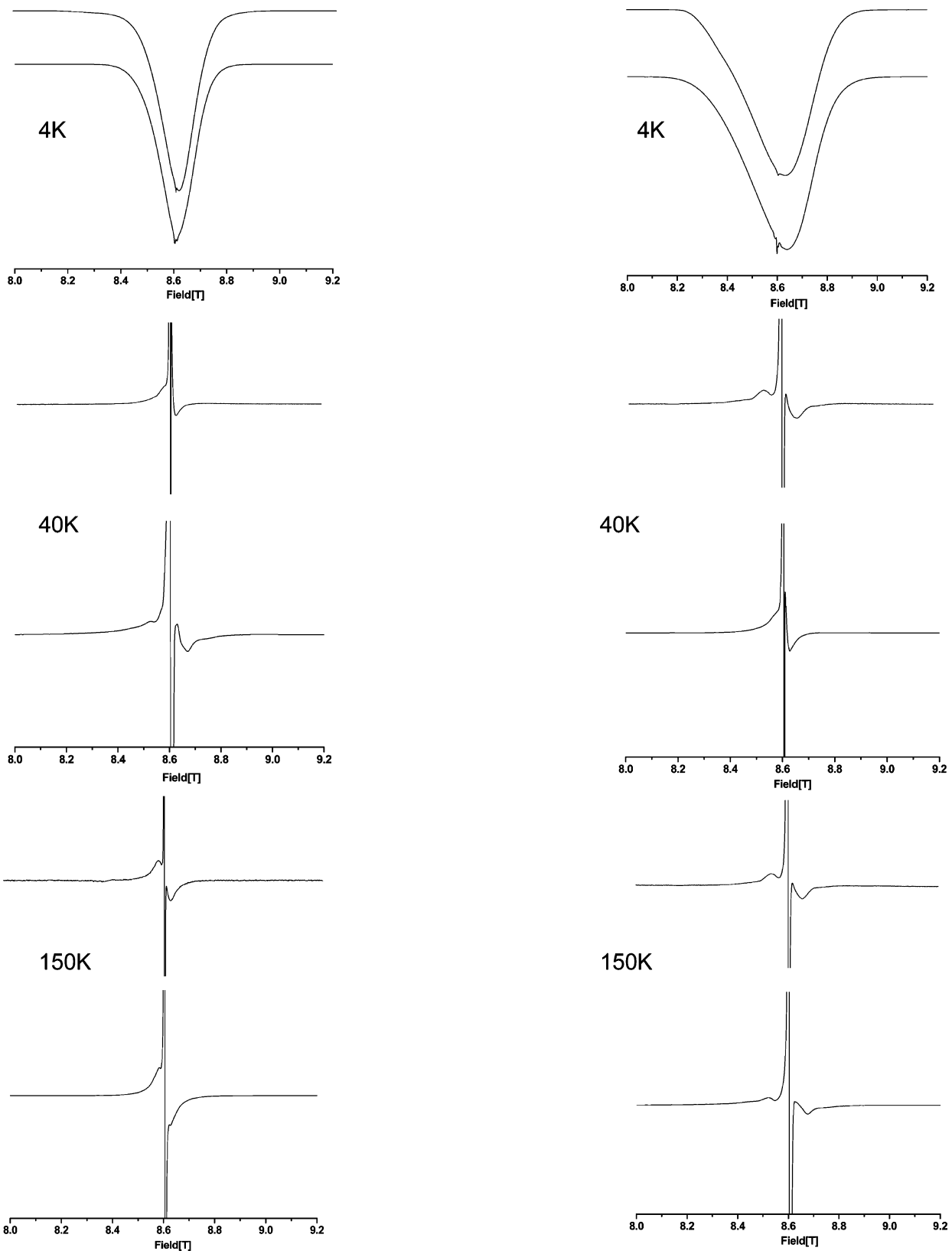

Figure 3. EPR spectra in water−glycerol glass for cyclic compounds at 4, 40, and 150 K: left, the experimental (upper) and the fitted (lower) spectra of $[Gd(DOTA)(H_2O)]^-$ glass; right, the experimental (upper) and the fitted (lower) spectra of Gd-P792(B) glass.

the same magnitude as D, with the exception of Gd-P792(R) (Table 2). The D and σD values of Gd-P792(B) are 3 times larger than that for $[Gd(DOTA)(H_2O)]^-$. Without surprise, all the ZFS parameters for $[Gd_2(p/m\text{X}(DO3A)_2)(H_2O)_2]$ are nearly equal. The *para* or *meta* substitution at the xylene group has no influence on the ZFS, and in accordance with the results for the acyclic binuclear complexes, no influence due to dipolar interaction between Gd(III) ions is observed. As could have been

Table 1. ZFS Parameters Obtained by Fitting the Experimental EPR Spectra at 4 K and 240 GHz for Acyclic Complexes. Estimated Error is 0.002 cm^{-1}

	D (cm^{-1})	E (cm^{-1})	σD (cm^{-1})	σE (cm^{-1})	E/D	g
$[Gd(DTPA)(H_2O)]^{2-}$	0.048	0.013	0.022	0.007	0.200	1.989
$[Gd_2(bipy\text{-}DTTA)(H_2O)_4]^{2-}$	0.055	0.016	0.024	0.009	0.290	1.989
$[Y_2/Gd_2(bipy\text{-}DTTA)(H_2O)_4]^{2-}$	0.054	0.016	0.027	0.007	0.300	1.989
$[Fe\{[Gd_2(bipy\text{-}DTTA)(H_2O)_4]\}_3]^{4-}$	0.056	0.016	0.020	0.006	0.290	1.989
$[Fe\{Y_2/Gd_2(bipy\text{-}DTTA)(H_2O)_4\}_3]^{4-}$	0.057	0.014	0.024	0.009	0.250	1.989
$[Gd_2Fe(tpy\text{-}DTTA)_2\ (H_2O)_4]$	0.050	0.014	0.037	0.006	0.280	1.989
$[Gd_2Ru(tpy\text{-}DTTA)_2\ (H_2O)_4]$	0.057	0.014	0.036	0.006	0.250	1.989

Table 2. ZFS Parameters Obtained by Fitting the Experimental EPR Spectra at 4 K and 240 GHz for Macrocyclic Complexes. Estimated Error is 0.002 cm^{-1}

	D (cm^{-1})	E (cm^{-1})	σD (cm^{-1})	σE (cm^{-1})	E/D	g
$[Gd(DOTA)(H_2O)]^{-}$	−0.019	0.000	0.019	0.013	0.0	1.989
Gd-P792(B)	−0.060	0.000	0.060	0.010	0.0	1.989
Gd-P792(R)	0.033	0.010	0.016	0.013	-	1.989
$[Gd_2(mX(DO3A)_2)(H_2O)_2]$	−0.038	0.006	0.033	0.023	0.160	1.990
$[Gd_2(pX(DO3A)_2)(H_2O)_2]$	−0.037	0.005	0.033	0.023	0.140	1.990

expected, in contrast to Gd-P792(B) and $[Gd(DOTA)(H_2O)]^{-}$, the E values of DO3A derivatives are nonzero. The lack of the fourth carboxylate arm in the DO3A ligand leads to a drop in the symmetry of the complex. However, it remains that the rhombicity factor E/D is smaller than that for the acyclic complexes. As it is well-known, the $[Gd(DOTA)(H_2O)]^{-}$ exists as two enantiomeric pairs of diastereoisomers in aqueous solution.[64,65] The two diastereoisomeric forms, labeled M (major) and m (minor) on the basis of the relative population in solution determined by NMR analysis, differ in the arrangement of the acetate arms. In the two isomers, the parallel squares, defined respectively by nitrogen and acetate oxygen atoms, are twisted by an angle of ca. 40° in M and −20° in m, providing a square antiprismatic and a twisted antiprismatic geometry, respectively. The increase in the molecular size for the P792(B) by substitution of hydrophilic arms may lead to a change on the M/m ratio and therefore a change of D. As it was mentioned in the Introduction, the Gd-P792(R) complex is characterized by six stereoisomers. A fit including six D and E as well as six σD and σE should be more appropriate for better determination of these parameters.

Comparison with Parameters from Solution. It is worthwhile to compare the values of the four ZFS parameters for $[Gd(DTPA)H_2O]^{2-}$ and $[Gd(DOTA)H_2O]^{-}$ to the previously calculated ZFS parameters in solution.[13,22] In the Rast et al. description, the transient ZFS modulation is described as an Ornstein−Uhlenbeck process,[39] namely, random diffusion over a Gaussian distribution. This can be regarded as a dynamic equivalent of the strain observed in the frozen solutions and described by σD and σE. It has been shown[30] that the ZFS parameter a_{2T} relevant for transient ZFS in relaxation studies in liquids is given by eq 3

$$a_{2T} = [2/3(\sigma D/2)^2 + 2(\sigma E/2)^2]^{1/2} \quad (3)$$

using the current definition of the strain parameters (full width at 0.6065 height of the Gaussian). The second-order static ZFS parameter a_2 has been calculated and is given by eq 4.

$$a_2 = [2/3(D)^2 + 2(E)^2]^{1/2} \quad (4)$$

Calculated a_2 and a_{2T} parameters for $[Gd(DOTA)H_2O]^{-}$ and $[Gd(DTPA)H_2O]^{2-}$ are reported in Table 3. The values of the static ZFS a_2 calculated from our glassy samples are similar to those obtained from relaxation studies in aqueous solution.[13,22] However, for both complexes, the calculated transient ZFS a_{2T} values are half of those obtained in solution. A possible reason could be that, instead of a dynamic process in solution, we consider a snapshot of this process in glasses. While there is likely a strong correlation between the static distribution of the microstructures in our flash frozen samples and the dynamical distribution in liquid aqueous solutions, we see that they are not identical.

^{1}H NMRD Profiles. Nuclear Magnetic Relaxation Dispersion (NMRD) is commonly used to measure the efficiency of Gd(III)-based MRI contrast agents. Theoretical description of NMRD profiles involves a very large number of parameters, including electronic relaxation parameters, more directly observed by EPR. An important progress in the analysis of NMRD was achieved by including variable temperature and frequency EPR data as described by Rast et al.[22] as well as ^{17}O NMR that mainly defines the water exchange rate and the rotational correlation time τ_R. The simultaneous analysis of experimental data of a different kind imposes more constraints on the parameters, which helps to solve the problem of the interdependence of parameters in NMRD analysis and yields physically meaningful values.[66] A further improvement of the analysis of NMRD profiles is now possible thanks to the independent determination of the ZFS parameters at low temperature and very high frequency as described above.

In the aim to show the importance of this approach, we use the ZFS parameters calculated from HF-EPR to fit ^{1}H NMRD profiles over the full frequency range (Figure 4) using a minimum of adjustable parameters by fixing as many of them as possible. The general procedure for the fit of NMRD profiles has been published elsewhere.[66] As Fries et al. have confirmed, the approximation of an effective monoexponential decay of the time correlation function (TCF) is valid for fast rotating

(64) Howard, J. A. K.; Kenwright, A. M.; Moloney, J. M.; Parker, D.; Woods, M.; Port, M.; Navet, M.; Rousseau, O. *Chem. Commun.* **1998**, *13*, 1381.
(65) Aime, S.; Botta, M.; Fasano, M.; Marques, M. P. M.; Geraldes, C. F. G. C.; Pubanz, D.; Merbach, A. E. *Inorg. Chem.* **1997**, *36*, 2059.
(66) Borel, A.; Yerly, F.; Helm, L.; Merbach, A. E. *J. Am. Chem. Soc.* **2002**, *124*, 2042.

Table 3. ZFS Parameters Determined by Rast Method in Solution in Comparison with the Parameters Obtained from Glasses for $[Gd(DTPA)H_2O]^{2-}$ and $[Gd(DOTA)H_2O]^{-}$

	$[Gd(DTPA)(H_2O)]^{2-}$		$[Gd(DOTA)(H_2O)]^{-}$	
	this work frozen solution[a]	Rast method aqueous solution[b]	this work frozen solution[a]	Rast method aqueous solution[b]
$a_2/10^{10}$ s^{-1}	0.80	0.92	0.30	0.35
$a_{2T}/10^{10}$ s^{-1}	0.22	0.43	0.23	0.43

[a] Calculated with the ZFS parameters D and E, σD and σE from Tables 1 and 2, according to the relations 3 and 4. [b] The previously calculated ZFS parameters a_2 and a_{2T} as published in ref 22.

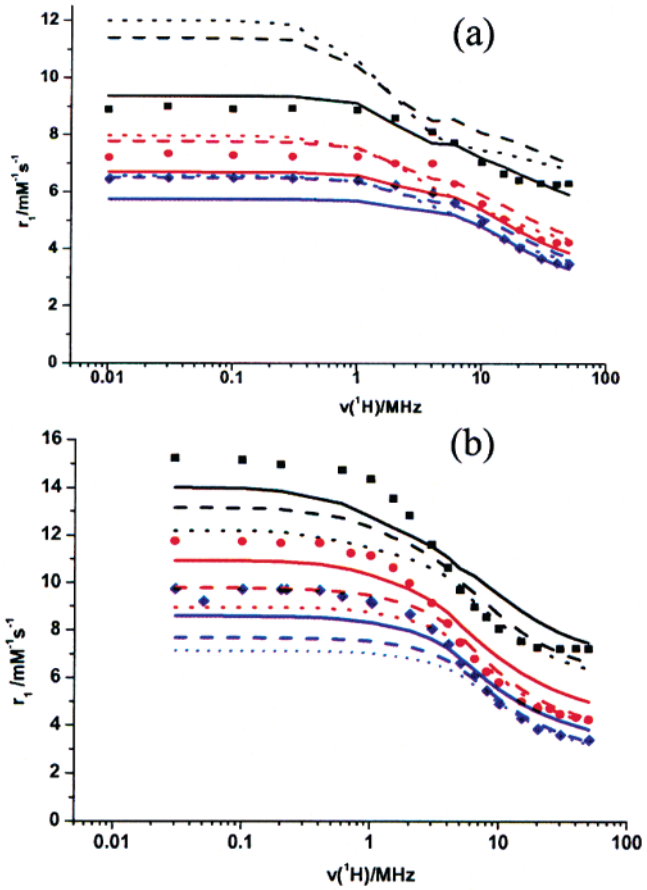

Figure 4. ^{1}H NMRD profiles of (a) $[Gd(DTPA)(H_2O)]^{2-}$ and (b) $[Gd(DOTA)(H_2O)]^{-}$. Experimental profiles are represented with symbols. In the calculated profiles represented with full lines, the four ZFS parameters determined in this work are fixed, and the four adjustable parameters (τ_{RO}^{298}, E_R, τ_v^{298}, and E_V) are free. In the simulated profiles represented with dashed and dotted lines, the ZFS parameters from ref 8 and those of this work are used, respectively. For both simulated profiles, the four adjustable parameters are fixed to the values from ref 8. The temperatures are from top to bottom: (a) 277, 298, and 308 K; (b), 277, 298, and 312 K, respectively.

complexes, such as $[Gd(DTPA)(H_2O)]^{2-}$ and $[Gd(DOTA)(H_2O)]^{-}$.[67]

The Matlab subroutine used for the calculations[15] was modified to allow nonaxial static (D, E) and transient (σD, σE) ZFS Hamiltonians, limited to 2nd order. These ZFS parameters are fixed in the fitting procedure as well as the water exchange rate (k_{ex}), and its activation enthalpy ($\Delta H^{\ddagger}$) is obtained from ^{17}O NMR experiments. The usual values of diffusion constant (D_{GdH}) and its activation energy (E_{DGdH}) as well as the Gd−water proton distances of the first (a_{GdHW1}) and second (a_{GdHW2}) coordination sphere are used.[10] The only remaining adjustable parameters for fitting experimental NMRD profiles are the global rotational correlation time of the Gd−O vector, τ_{RO} (related by a constant factor of 0.65 to τ_{RH}),[10] and its activation energy, E_R, and the so-called vibrational correlation time, τ_v, and its activation energy, E_v. We extended the calculations to the low-field region, where the electronic relaxation plays an important role by using the Monte Carlo approach.[15] The results of the fits for $[Gd(DTPA)(H_2O)]^{2-}$ and $[Gd(DOTA)(H_2O)]^{-}$ (experimental data, ref 10) are reported in Table 4 and Figure 4.

Table 4. Parameters Obtained for NMRD Profiles of $[Gd(DTPA)(H_2O)]^{2-}$ and for $[Gd(DOTA)(H_2O)]^{-}$ by Introducing the Fixed ZFS Parameters Calculated from HF-EPR[a]

	$[Gd(DTPA)(H_2O)]^{2-}$	$[Gd(DOTA)(H_2O)]^{-}$
$k_{ex}^{298}/10^6$ s^{-1}	3.8	4.6
$\Delta H^{\ddagger}$/kJ mol^{-1}	52.9	54.5
$D_{GdH}^{298}/10^{-10}$ m^2 s^{-1}	23.0	23.0
E_{DGdH}/kJ mol^{-1}	17	18.1
$\tau_{RO}^{298}/10^{-12}$ s	80 (115)	149 (100)
E_R/kJ mol^{-1}	13.6 (20.0)	20.0 (20.0)
τ_{RH}/τ_{RO}	0.65	0.65
$\tau_v^{298}/10^{-12}$ s	0.29 (0.10)	0.42 (0.65)
E_v/kJ mol^{-1}	0.5 (1.0)	8.6 (8.6)
$a_{GdHW\,1}$/Å	3.1	3.1
$a_{GdHW\,2}$/Å	3.5	3.5
a_{Gd-O}/Å	2.5	2.5
D (cm^{-1})	0.048	−0.019
E (cm^{-1})	0.013	0
σD (cm^{-1})	0.022	0.019
σE (cm^{-1})	0.007	0.013
g	1.99	1.99

[a] Underlined parameters were fixed to values from ref 10 in the fit. The D, E, σD, and σE values are fixed in the fit. The four parameters in parentheses are those from ref 8. The τ_{RH}/τ_{RO} ratio is considered as a common value for the ratio of the two rotational correlation times.[24]

In this figure, we compare the NMRD profiles calculated in various ways with the experimental ones. The simulated profiles with the ZFS parameters, a_2, a_4, a_6, and a_{2T}, determined in solution[10] are presented with dotted lines. The dashed lines represent NMRD profiles simulated by replacing the ZFS parameters by D, E, σD, and σE determined in this work. The use of these last parameters leads to a slight improvement in the low-field range of the simulated NMRD profiles for both complexes. The result of the fit with the four adjustable parameters is represented with full lines. As expected, a significant improvement is observed for both complexes. The value of τ_{RO} extracted from the fit in the case of $[Gd(DTPA)(H_2O)]^{2-}$ is reasonable but too long for $[Gd(DOTA)(H_2O)]^{-}$, a molecule of similar size. An explanation can be that ^{17}O NMR data which impose constraints on the variation of τ_{RO} were not included in our fit. The most reasonably reproduced NMRD profiles are probably the simulated ones (dashed lines) with the ZFS parameters D, E, and their distributions, representing the best result at frequencies above 5 MHz. Further improvement might be achieved by including 4th and 6th order terms (either the mean magnitude parameters a_4 and a_6 or the individual components of the tensors). However, the broad, featureless nature of our experimental spectra would hamper an unambiguous determination of additional higher order parameters.

On the basis of our fitting results, further simulations were carried out to evaluate the effect of rhombicity of the static and

(67) Fries, P. H.; Belorizky, E. *J. Chem. Phys.* **2005**, *123*, 124510-1.

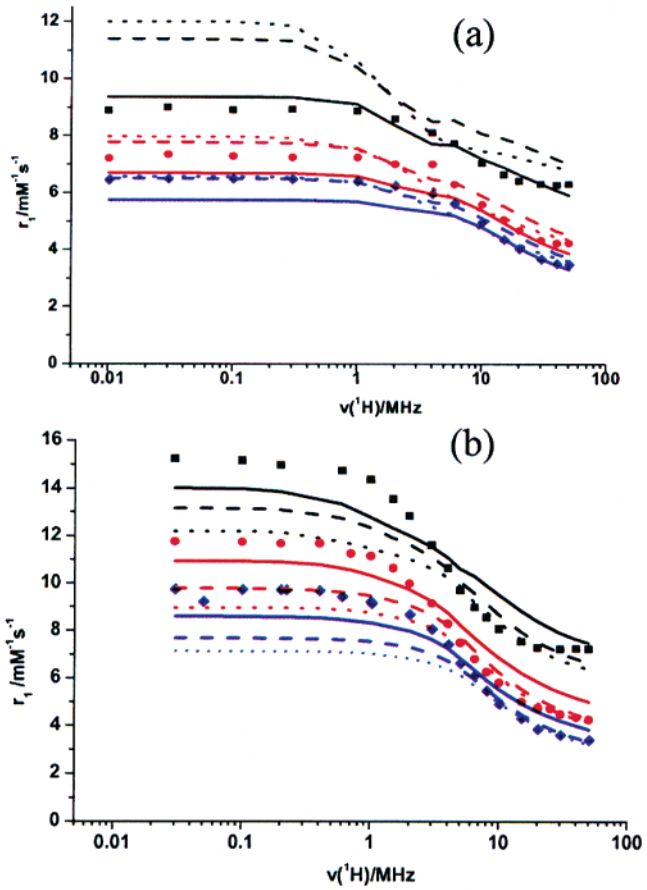

Figure 5. ^{1}H NMRD profiles of (a) $[Gd(DTPA)(H_2O)]^{2-}$ and (b) $[Gd(DOTA)(H_2O)]^-$; experimental profiles are represented with symbols, calculated profiles with full lines and simulated profiles with E/D equal to zero for $[Gd(DTPA)(H_2O)]^{2-}$ and σE equal to zero for $[Gd(DOTA)(H_2O)]^-$ with dashed lines. The temperatures are from top to bottom: (a) 277, 298, and 308 K; (b), 277, 298, and 312 K, respectively.

the transient ZFS on the NMRD profile. Kowalewski and coworkers[68] included rhombicity in both the transient and the static part of the ZFS in their slow motion theory to analyze experimental NMRD profiles of several low symmetry Ni(II) complexes at low-field range. They showed that rhombicity in the transient ZFS is of central importance for the electron spin dynamics. In our study of Gd(III) complexes, we first applied a variation of ±20% on the value of ZFS parameter D, which leads only to minor changes on the NMRD profiles for both complexes. For $[Gd(DTPA)(H_2O)]^{2-}$, by setting the static ZFS rhombicity to zero ($E = 0$), we observe a notable influence on the NMRD profiles at low frequency (dashed lines in Figure 5a). However, due to the large static ZFS, setting the transient part of the ZFS to zero (σD and/or $\sigma E = 0$) has no effect on the simulated nuclear spin relaxation curves. For $[Gd(DOTA)(H_2O)]^-$, the magnitude of the static ZFS is lower than that for $[Gd(DTPA)(H_2O)]^{2-}$, and therefore more influence of the transient ZFS should be expected. As there is no rhombicity of the static ZFS part (E is already equal to zero), we set σE to zero. We notice a small increase of nuclear spin relaxation at low field corresponding to slower effective electronic relaxation (dashed lines in Figure 5b). Thus, we see that the static ZFS rhombicity has stronger influence on the low-field relaxivity than that of the transient ZFS.

(68) Nilsson, T.; Parigi, G.; Kowalewski, J. *J. Phys. Chem. A* **2002**, *106*, 4476.

Conclusions

The present EPR investigations on a frozen solution of several Gd(III)-based contrast agents for MRI have been carried out to determine the zero-field splitting parameters. The very high frequency EPR study combined with very low temperature measurements constitutes a direct method to determine the magnitude and unequivocally the sign of the static ZFS parameter D as well as its rhombicity E and their distributions σD and σE. These two latter parameters correlate with the transient ZFS part, which is important to describe electronic spin relaxation in solution. The EPR spectra presented indicate a correlation between the sign of D and the nature of the chelate structure surrounding the Gd(III): a positive sign was observed for all the acyclic complexes and a negative one for the macrocyclic complexes. For the first time, we show experimentally that the lower symmetry of $[Gd(DTPA)(H_2O)]^{2-}$-type complexes as compared to that of $[Gd(DOTA)(H_2O)]^-$-type complexes is reflected by a larger rhombicity of the static ZFS for the first ones. Direct measurements of ZFS parameters in glasses and comparison with those previously obtained from tedious multifrequency and variable temperature EPR measurements in solution show good agreement for the static ZFS. This good agreement allowed us to use these ZFS parameters to simulate NMRD profiles over the whole frequency range by including dynamics parameters (k_{ex}, τ_{RO}) determined by ^{17}O NMR experiments. In this way, the number of adjustable parameters in the fitting of NMRD profiles is strongly reduced. Another advantage of the direct determination of the ZFS terms is the availability of the rhombicity of the static and transient ZFS parameters (E, σE) which allows the study of their influence on the low-field ^{1}H relaxivity, where the electronic relaxation mechanism plays an important role.

Acknowledgment. The Program Enhancement Grant 01-05 from the FSU Foundation to the NHMFL EMR program is acknowledged for financial support. This work is also supported by the Swiss National Science Foundation and the Swiss state Secretariat for Education and Research (SER). This research was carried out in the frame of the EU COST Action D18 and European founded EMIL program LSHC-2004-503569.

Supporting Information Available: Tables of calculated line widths, figures of experimental and simulated EPR spectra at 240 GHz and 4, 40, and 150 K for $[Gd_2M(tpy\text{-}DTTA)_2(H_2O)_4]$ ($M^{II} = Fe^{II}$, Ru^{II}), Gd-P792(R), $[Y_2/Gd_2(bipy\text{-}DTTA)(H_2O)_4]^{2-}$, and $[Fe\{Y_2/Gd_2(bipy\text{-}DTTA)(H_2O)_4\}_3]^{4-}$. Figures of experimental and simulated NMRD profiles for $[Gd(DTPA)(H_2O)]^{2-}$ and $[Gd(DOTA)(H_2O)]^-$. This material is available free of charge via the Internet at http://pubs.acs.org.

JA0583261